Shifting-reference concentration cells to refine composition-dependent transport characterization of binary lithium-ion electrolytes

Andrew A. Wang [a], Tianhong Hou [a], Minnie Karanjavala [a], Charles W. Monroe [a, b, *]

[a] *Department of Engineering Science, University of Oxford, Parks Road, Oxford, OX1 3PJ, United Kingdom.*

[b] *The Faraday Institution, Harwell Campus, Didcot, OX11 0RA, United Kingdom.*

* Corresponding Author – Email: charles.monroe@eng.ox.ac.uk

ABSTRACT

We present a novel 'shifting-reference concentration-cell' method, altering the traditional protocol for measuring liquid-junction potentials by using a sequence of reference concentrations in regularly spaced intervals, rather than a fixed reference. The method, applied to solutions of lithium hexafluorophosphate ($LiPF_6$) in propylene carbonate (PC) and ethyl methyl carbonate (EMC) at 25 °C, helps to determine thermodynamic factors more accurately, and is useful across a wider concentration range. For $LiPF_6$:PC, good agreement with prior fixed-reference measurements is shown, and new data at low concentrations is consistent with Debye–Hückel theory. Original composition-dependent property correlations are produced for $LiPF_6$:EMC up to 2 M, including the density and thermodynamic factor, as well as isothermal-transport properties such as transference number, conductivity, diffusivity, and viscosity. Polarization-relaxation simulations validate these correlations. For $LiPF_6$:EMC, the low thermodynamic factor and cation/anion Stefan–Maxwell diffusivity, as well as Walden analysis, suggest that ion association dominates, even at high dilution.

1. Introduction

Although it may be possible to improve the performance of lithium-ion batteries by altering their electrolytes, the possibilities afforded by liquid-electrolyte design remain unclear. More complete and accurate parameterization of thermodynamic and transport properties can be used in conjunction with phenomenological models to shed light on how electrolyte composition affects cell efficiency, degradation, and power capability.

The widely adopted concentrated-solution theory [1] describes solution-phase mass-transport phenomena in electrochemical cells. For a simple binary electrolyte, the theory involves three macroscopic transport parameters – ionic conductivity, cation transference number, and thermodynamic diffusivity – which derive from parameters that describe microscopic species/species interactions. As well as these dynamical properties, the description of a binary electrolyte requires a thermodynamic factor and partial molar volumes for salt and solvent, which together describe the electrolyte's equilibrium state.

Thermodynamic factors express how concentration variation within an electrolyte translates into the open-circuit voltage drop across it. They relate closely to activity coefficients, measuring deviation of the chemical (or electrochemical) potential of a species from ideal-mixing behavior [2]. Activity-coefficient data for nonaqueous electrolytes is not abundant, although direct measurement of thermodynamic factors *via* colligative properties (melting-point depression) [3] has been performed by Stewart and Newman [4] for lithium-battery electrolytes. It has been more common to use concentration-cell experiments – which measure liquid-junction potentials between a test and reference electrolyte in electrochemical contact – to determine a property that convolutes the thermodynamic factor with a transference number. Most concentration-cell analyses assume the transference number to be constant, or use model-dependent numerical

optimization to deconvolute the transference number and thermodynamic factor, introducing unwanted uncertainties [4–8]. All prior concentration-cell studies have employed fixed, arbitrary reference concentrations, which can introduce inaccuracies when measuring highly dilute or concentrated test concentrations [4–14].

The thermodynamic factor χ of a binary electrolyte is defined in terms of the solvent chemical potential μ_0, through the relation [15]

$$y_0 \vec{\nabla} \mu_0 = -\nu R T \chi \vec{\nabla} y, \tag{1}$$

where R is the universal gas constant, T is the absolute temperature, and $\nu = 2$ is the number of ions in a formula unit of $LiPF_6$. Here y is the salt particle fraction, which is convenient to describe composition when considering solute-volume effects [15]; particle fractions are similar to mole fractions, but are based on a measure of total molar content in which each ion is considered as a separate species. In a binary solution, the solvent particle fraction y_0 relates to y through the phase rule $y_0 + \nu y = 1$.

Through the isothermal, isobaric, locally electroneutral Gibbs–Duhem equation, χ can be understood as a Darken factor [16], which expresses how the salt's activity in the liquid varies with its concentration. In terms of salt activity coefficients [1,15,17], χ can be written as

$$\chi = 1 + \left(\frac{\partial \ln \lambda_{+-}}{\partial \ln y}\right)_{T,p} = \frac{1}{y_0}\left[1 + \left(\frac{\partial \ln \gamma_{+-}}{\partial \ln m}\right)_{T,p}\right] = \frac{\bar{V}_0}{y_0}\left[1 + \left(\frac{\partial \ln f_{+-}}{\partial \ln c}\right)_{T,p}\right], \tag{2}$$

in which $\bar{V}_0$ is the partial molar volume of solvent, m is salt molality and c is salt molarity; λ_{+-}, γ_{+-}, and f_{+-} respectively represent mean molar salt activity coefficients over particle-fraction, molal, and molar bases.

Below we introduce the shifting-reference concentration-cell method, an approach to diffusion-potential measurement that minimizes the difference between reference and test

concentrations across the studied composition range, thereby mitigating the intrinsic error associated with convoluting the composition dependences of the thermodynamic factor and transference number, as well as maintaining a good signal-to-noise ratio in highly dilute or concentrated regimes. The method is validated against fixed-reference concentration-cell data for lithium hexafluorophosphate ($LiPF_6$) in propylene carbonate (PC), and also carried out for $LiPF_6$ in ethyl methyl carbonate (EMC). The thermodynamic factor is isolated using transference-number correlations obtained by applying the Hittorf method presented by Hou and Monroe [12]. Additional transport and thermodynamic property characterization from 0 to 2.5 M for $LiPF_6$ in EMC complements the thermodynamic-factor measurement. It also allows quantification of the three Onsager–Stefan–Maxwell diffusivities, which parameterize interspecies diffusional drag forces in solution. Viscosity data for both $LiPF_6$:PC and $LiPF_6$:EMC are also reported, to underpin Walden analyses that give further insight about ion pairing. Taken together, the data suggest that $LiPF_6$:PC behaves as a typical strong electrolyte, whereas $LiPF_6$:EMC is weak.

A suite of techniques that includes the shifting-reference concentration-cell method can be applied to both strongly and weakly dissociated electrolytes. The results reported below highlight how ion association can impact the composition-dependent transport and thermodynamic properties of binary electrolytes.

2. Experimental

2.1 Electrolyte preparation

All solutions were prepared in a temperature-controlled (25.0 ± 0.5 °C), argon-filled glovebox (Inert Technologies) with sub-ppm H_2O and O_2 levels. Fresh containers of $LiPF_6$ salt (99.99%, battery grade, Sigma Aldrich) were first opened inside the glovebox; the salt was

vacuum dried in a heated antechamber for 24 hours at 60 °C. EMC and PC solvents (99.9%, anhydrous, Sigma Aldrich) were dried using 3 Å molecular sieves in the glovebox for a week before use. Karl Fischer titration was performed on prepared electrolytic solutions, in which the water content was determined to be less than 10 ppm.

2.2 Densitometry and composition

Electrolyte standards for density/composition correlations were prepared gravimetrically with given salt mass fractions ω, according to procedures described by Hou and Monroe [12]. Measurements of density ρ were performed using a high-precision oscillation density meter (DMA4100, Anton Paar) inside the glovebox. The apparatus quantifies density with five-digit precision and controls temperature within ±0.02 °C. Densities that were used to produce composition correlations were measured in triplicate at 20.0, 25.0, and 30.0 °C.

Salt molarity c relates to mass fraction and density through

$$c = \frac{\omega\rho}{M_\mathrm{e}}, \tag{3}$$

where M_e is the molar mass of $LiPF_6$ (151.905 $\mathrm{gmol^{-1}}$). For a binary electrolyte, partial molar volumes of solvent and salt can also be calculated using a density/molarity correlation [1], a process which is also described in Appendix A1.

In terms of species molarities, $y = c/(c_+ + c_- + c_0)$, where subscripts +, –, and 0 respectively denote cations, anions, and solvent. In locally electroneutral binary electrolytes, salt particle fraction can be written in terms of salt molarity or mass fraction as

$$y = \frac{M_0 c}{\rho + (\nu M_0 - M_\mathrm{e})c} = \frac{M_0\omega}{M_e + (\nu M_0 - M_\mathrm{e})\omega}, \tag{4}$$

where M_0 is the molar mass of solvent (104.105 $\mathrm{gmol^{-1}}$ for EMC and 102.089 $\mathrm{gmol^{-1}}$ for PC).

2.3 Viscometry

Dynamic viscosity η was measured with an in-line rolling-ball viscometer attachment to the densitometer (Lovis 2000, Anton Paar). A capillary with a 1.59 mm diameter was used for viscosity measurements across the same concentration range probed by densitometry, at temperatures of 20.0 ± 0.02, 25.0 ± 0.02, and 30.0 ± 0.02 °C.

2.4 Hittorf experiment

Cation transference number relative to the solvent velocity, t_+^0, was measured with a custom-made gravimetric Hittorf cell. A detailed theoretical analysis of the Hittorf experiment, a derivation of equation 5, and schematic diagrams of the experimental cell were provided previously by Hou and Monroe [12].

The Hittorf cell has two configurations, designated ‘open’ and ‘closed’. In the open configuration, the cell contains a single cylindrical cavity, whose ends are terminated by lithium metal electrodes. Two stopcocks can be turned to put the cell into the closed configuration, wherein the central cavity is segmented into anodic, neutral and cathodic chambers of known volume, which can be separately drained through access plugs.

To perform the Hittorf experiment, lithium was prepared by polishing lithium foil (99.9% Alfa Aesar) with a PTFE brush to remove any trace oxidized surface layer, punched into discs, and placed on either end of the Hittorf cell. Current-collector endcaps were screwed on to hold the lithium discs in place and seal the central cavity. Then, the stopcocks were set in the open configuration and electrolyte of known density was loaded in through the access plugs, which

were subsequently sealed. Finally, the cell was oriented vertically, and a constant current I_{pulse} = 0.2 mA was passed for duration T_{pulse} = 20 hours with a potentiostat/galvanostat (PGSTAT302N, Metrohm). During the current flow, lithium is plated onto the cathode and stripped from the anode, inducing a concentration difference across the central chamber. The magnitudes of I_{pulse} and T_{pulse} were selected such that the concentration boundary layers remained within the anodic and cathodic chambers during the experimental period [18]; the total charge passed was restricted below 20 C (translating to an areal charge of *ca.* 7 mAh•cm^{-2}) to minimize the possibility of side reactions [2]. Immediately after the current was cut off, the stopcocks were set to the closed configuration, and solutions extracted from the sealed chambers were stirred for 2 h to homogenize their concentrations. Densities of these solutions were measured at 25 °C, and their molarities were found by inverting the density/molarity correlation $\rho_{25°C}(c)$ established by densitometry. Then, t_+^0 was calculated from

$$t_+^0 = 1 - \frac{FV_{\text{chamber}}|c_{\text{f}} - c|}{I_{\text{pulse}}T_{\text{pulse}}(1 - \bar{V}_{\text{e}}c)}, \tag{5}$$

a Hittorf formula derived under the assumption that lithium ions are the only liquid-phase species which reacts at the electrodes. Here $V_{\text{chamber}} = 4.0 \pm 0.1$ mL is the volume the cathodic or anodic chamber, c_{f} is the concentration of the homogenized solution extracted from said chamber, c is the initial concentration of the sample, and $\bar{V}_{\text{e}}$ is the salt partial molar volume at c, calculated from the density correlation *via* equation A1 in appendix A.

2.5 Shifting-reference concentration cells

Concentration cells place electrolytes containing similar molecular species with two different compositions in chemical contact: these are called the 'reference' solution, with composition y_{ref}, and the 'test' solution, y_{test}. A porous grade D frit (10–16 μm) between the

electrolytes impedes diffusion across the cell, as depicted in figure 1(a). The difference in salt chemical potential across the frit results in a measurable liquid-junction potential ΔU. For a concentration cell in which the electrodes are reversible only to cations, ΔU is a functional of salt composition y through the thermodynamic factor χ and transference number t_+^0 [1,4,12],

$$\Delta U = \frac{\nu RT}{F} \int_{y_{\mathrm{ref}}}^{y_{\mathrm{test}}} \chi(1 - t_+^0) d \ln y. \tag{6}$$

Writing equation 6 in terms of properties correlated to the salt-fraction composition basis obviates the need for excluded-volume corrections, simplifying the integrand considerably [15].

Traditional concentration-cell studies employ a single reference composition across all test compositions. The use of a single reference composition can lead to issues, however. Although the thermodynamic factor χ is a state function, dependent only on the (presumably constant) surface concentrations at the electrodes, the integral in equation 6 also involves the composition dependence of t_+^0. Furthermore, when differences between y_{test} and y_{ref} are large, a steady voltage plateau may never arise because the diffusion driving forces are larger, causing large transient variation of concentration profiles that incurs a concomitant change in t_+^0 with time. This has been confirmed experimentally in some studies of concentrated electrolytes, which have shown that the dependence of liquid-junction potentials on integral averages of transference numbers can be problematic [8,19]. Problems occur in the dilute regime as well: if y_{test} is close to 0, the natural dependence of ΔU on $\ln y$ means that small variation in test concentrations can result in very large voltage changes if the reference composition is fixed.

The shifting-reference concentration-cell approach employs a matrix of liquid-junction potentials banded about a variable reference composition, minimizing the concentration difference across the liquid junction to mitigate potential errors due to local t_+^0 variation. By measuring two test compositions y_{test} above and below each reference composition y_{ref}, a band of several

concentration-cell measurements (five in the present case) can be fit by a function describing $\Delta U(y)$, which can subsequently be used to interpolate the derivative of the liquid-junction potential with respect to composition at y_{ref}, removing the need to involve the integral that appears in equation 6.

By direct differentiation of equation 6 with respect to the test concentration, Newman [1] showed that

$$\chi(1-t_+^0) = \frac{F}{\nu RT}\left(\frac{d\Delta U}{d\ln y}\right) = \frac{Fy}{\nu RT}\left(\frac{d\Delta U}{dy}\right). \tag{7}$$

Thus a differential measurement of $\chi(1-t_+^0)$ can be found by interpolating a local value of $d\Delta U/dy|_{y_{\mathrm{ref}}}$ – the change in liquid-junction potential with respect to composition at the reference composition. To analyze data, we assume $d\Delta U/d\ln y$ can be fit by a second-order polynomial, so that

$$\frac{d\Delta U}{dy} = \frac{U_1 + U_2 y + 2U_3 y^2}{y}. \tag{8}$$

Integration of this expression with respect to composition produces a function that can be fit directly to experimental liquid-junction-potential data.

When repeated for multiple y_{ref} values across the concentration range, the method produces a distinct value of $\chi(1-t_+^0)$ at each composition y_{ref}. Thus the method produces a differential measurement with respect to composition, rather than a measurement involving an integral that convolutes the composition dependences of χ and t_+^0.

Figure 1(b) illustrates the qualitative differences between shifting-reference and fixed-reference concentration-cell data sets, with the surface of banded liquid-junction potentials (red) more closely applying the differential form of equation 6 embodied by equation 7. In principle it is possible to fit a 2-dimensional surface to the data obtained with the shifting-reference method.

Resolution in a narrow band of ΔU due to smaller composition differences was found to result in highly variable surface fits, however, so a band of concentrations around $y_{test} = y_{ref}$ was fit to produce a $\chi(1 - t_+^0)$ for each y_{ref}. The number of individual experiments can also be halved by noting that y_{ref} and y_{test} can be interchanged in the matrix of ΔU measurements.

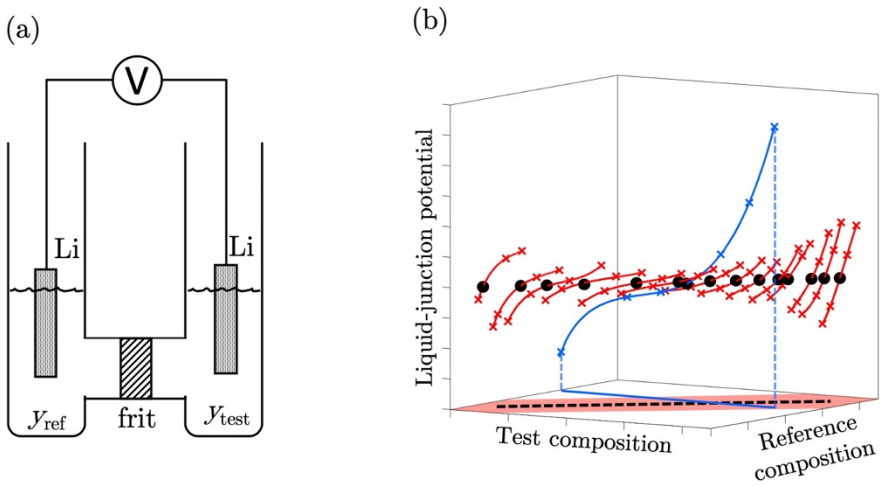

Figure 1. (a) Schematic of the glass 'H' shaped concentration cells. (b) Surface of shifting-reference concentration-cell measurements (red) and single reference concentration cell method (blue). Reference concentrations are demarcated with dots (•) and test concentrations, with crosses (x).

Inside the temperature-controlled glovebox, 5.0 mL samples of test and reference electrolytes were simultaneously pipetted into each chamber of the glass H-cell. Lithium foil was prepared as described in section 2.4 before being cut into strips and submerged in each chamber to act as symmetric, reversible reference electrodes. After allowing the liquid-junction potential to stabilize over 1 hour in the glovebox at 25 °C, the steady-state open-circuit potential was recorded with a potentiostat (PGSTAT302N, Metrohm). Reference concentrations of $LiPF_6$:PC were varied in increments of approximately 0.1 M from 0.1 to 2.5 M, and test concentrations were targeted at ±0.1, ±0.2 M intervals around the reference concentration. Increments for $LiPF_6$:EMC were larger to improve voltage resolution of the potentiostat measurement, with 0.2 M reference spacing from

0.2 to 2 M and ±0.2, ±0.4 M test-concentration bands. Additional shifting-reference concentration-cell measurements were performed at lower concentrations — spaced evenly in $\sqrt{y}$ to match expectations based on Debye and Hückel's infinite-dilution limiting law — for both $LiPF_6$:PC and $LiPF_6$:EMC binary electrolyte systems. All liquid-junction potentials were measured in triplicate.

2.6 Ionic conductivity

Ionic conductivity κ was measured with an AC conductivity probe (Orion A212, Thermo Scientific) in a sealed cell placed in a temperature-controlled water bath, following the procedure described in reference [12]. Bulk resistances for cells with separators were obtained by electrochemical impedance spectroscopy (EIS) using an impedance module embedded in the potentiostat/galvanostat (Octostat5000, Ivium Technologies). This data was used to obtain MacMullin numbers (geometric factors), which subsequently were used to correct restricted-diffusion measurements for the effects of porous separators, as described by Hou and Monroe [12]. Macmullin numbers and Bruggeman factors are presented in figure S2 of the supplementary information that accompanies this article.

2.7 Restricted diffusion

The Fickian diffusivity *D* can be measured in a restricted-diffusion experiment, wherein the relaxation of a nonuniform concentration distribution in a confined volume of electrolyte is tracked by monitoring the decay in concentration polarization between two fixed points. Thompson and Newman demonstrated that irrespective of the initial nonuniform concentration profile, the exponential decay in polarization follows Fick's second law $\left(\frac{\partial c}{\partial t} = D\frac{\partial^2 c}{\partial x^2}\right)$, and will occur for relaxation timescales $t > \frac{0.05L^2}{D}$, where L is the length of the cell [20]. Transient

concentration gradients can be tracked voltammetrically using open-circuit-potential (OCP) measurements between two identical reference electrodes. For small enough concentration gradients, the OCP will be directly proportional to concentration differences [11,18,21].

A planar, parallel-electrode symmetric cell was assembled by sandwiching an annular polyether ether ketone (PEEK) spacer (thickness: L=2.00 mm, inner diameter: 8.00 mm, outer diameter: 16.00 mm) between two lithium discs. These discs were punched from lithium foil that was roller pressed such that the foil thickness was approximately 0.6 mm as measured *via* micrometer gauge. The spacer gap was filled with electrolyte in an inert glass-fiber separator (FisherBrand, porosity $\varepsilon = 0.85$) to minimize the effects of externally induced vibrations and lithium malleability. This cell sandwich was sealed in a coin cell (CR2032, MTI) using a pneumatic crimper at 380 kPa. The consistency in sealing pressure, cell dimension, and lithium disc dimensions further mitigates error introduced by possible lithium deformation.

Linear fits of $-\ln(\mathrm{OCP})$ *vs.* time were performed, and the slope was used to determine an effective Fickian diffusivity D_{eff}:

$$\lim_{t\to\infty} \frac{d\ln(\mathrm{OCP})}{dt} = -\frac{\pi^2 D_{\mathrm{eff}}}{L^2 \varepsilon}, \tag{9}$$

where D_{eff} and porosity ε account for the effective diffusivity of solution in the porous separator medium. Concentration gradients were introduced by potentiostatically holding the cell at 100 mV for 12 hours (Octostat5000, Ivium Technologies). Once a steady-state current was reached, the current was shut off and OCP relaxation was recorded. The potentiostatic hold and its duration were chosen such that the OCP achieved immediately after the initial capacitive relaxation of cell voltage remained below 50 mV, a range within which the relationship between OCP and

concentration polarization is more linear [18]. Experiments were all performed by placing the apparatus in a thermal chamber (Binder) at 25.0 °C.

3. Results and discussion

3.1 Density and composition

Density data is plotted as a function of salt molarity in figure 2. A correlation was produced following Hou and Monroe [12], using a functionality in line with Debye–Hückel theory that also minimizes confidence intervals on the parameters:

$$\rho = \rho_0 + \rho_1 c + \rho_2 c^{3/2}. \tag{10}$$

Thermodynamics allows that parameters ρ_0, ρ_1, and ρ_2 may vary with temperature and pressure. Correlations in this form for $LiPF_6$:PC were reported previously [12]; parameters for $LiPF_6$:EMC at 20, 25, and 30 °C are provided in table 2.

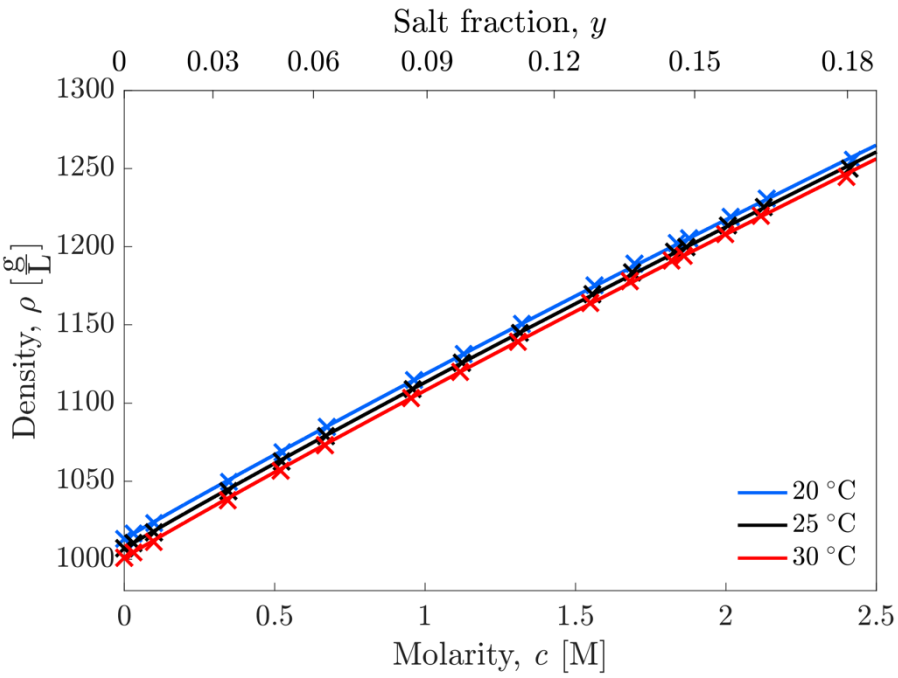

Figure 2. Density/composition measurements for $LiPF_6$:EMC (x) and correlations from equation 10 (—) at 20 °C (blue), 25 °C (black), and 30 °C (red).

Partial molar volumes of salt $\overline{V}_e$ and solvent $\overline{V}_0$ for $LiPF_6$:EMC were determined using equation A1 of the appendix. The variation of these properties was similar to previous observations for $LiPF_6$:PC [12] in the 0–2.2 M range, with $\overline{V}_e$ increasing comparatively more (~33.5%) than the decrease in $\overline{V}_0$ (~1%). Raw density data are tabulated in table S1 in the supplementary information that accompanies this article.

3.2 Transference number

The cation transference number with respect to the solvent velocity, t_+^0, is plotted in Figure 3 for various Hittorf experiments at 25 °C. Results from both the anodic and cathodic chambers of the Hittorf cell were gathered, and the combined data set was fit with a second-order polynomial, yielding the correlation

$$t_+^0 = 0.4130 - 1.551y + 3.942y^2 \quad (11)$$

for $LiPF_6$:EMC solutions. The Hittorf transference number t_+^0 decreases monotonically with increasing concentration, from Li^+ carrying approximately 40% of the total charge ($t_+^0 \approx 0.4$) near infinite dilution to approximately 25% at 2.5 M. Raw data from the Hittorf experiments are presented in table S2.

Note that the Hittorf formula, equation 5, was derived under the assumption that the electrolyte is a three-species system comprising a single positive species, a single negative species, and a neutral solvent [12,15]. There is widespread discussion in the literature about possible speciation of the lithium salt, into (say) solvent-coordinated ions, neutral ion pairs, charged ion aggregates such as Li_2X^+ or LiX_2^-, or even solvent-coordinated polyionic superstructures [22,23]. Since each of these secondary structures is formed by local

association/dissociation reactions involving lithium cations, hexafluorophosphate anions, and solvent molecules, the electrochemical potentials of said structures are linearly dependent on those of the primary species in an equilibrium state. Therefore, if the timescale for reaching speciation equilibrium is fast compared to the timescale for salt diffusion, a three-species model can still be applied to systems with significant speciation, but the interpretation of the parameters needs to be relaxed. In cases where speciation is appreciable, the number t_+^0 should be interpreted as a measure of the net drift of all the Li-containing species, relative to a reference frame set by the velocity of free solvent molecules. This issue has been discussed in more detail by Onsager [24], Newman [1], and Lacey [25]; the presence of speciation equilibria can justify surprising experimental observations such as negative transference numbers [14].

Figure 3 also shows the cation transport number t_+ (the Bruce–Vincent transference number [26]), which is obtained if the Hittorf experiment is analyzed with a model that ignores solute-volume effects, such as Nernst–Planck dilute-solution theory [12] or a concentrated-solution theory that neglects the salt's partial molar volume [27]. Since the apparent t_+ value is influenced by Faradaic convection, it varies with applied current; by contrast, t_+^0 is a truly isolable bulk property of an electrolytic solution. The validity of equation 5 also requires that only cations react at the electrode in the half-cell being modelled, in which case t_+^0 relates to t_+ through the volume fraction of salt, $c\overline{V}_\mathrm{e}$,

$$t_+ = 1 - (1 - t_+^0)(1 - c\overline{V}_\mathrm{e}). \qquad (2)$$

The terms in equations 5 and 12 proportional to the solvent volume fraction, $(1 - c\overline{V}_\mathrm{e})$, correct Hittorf's standard formula to account for the displacement of solvent volume by salt as interfacial reactions progress. This phenomenon has been analyzed previously by Lindberg et al. [6,7] and Monroe et al. [12,15].

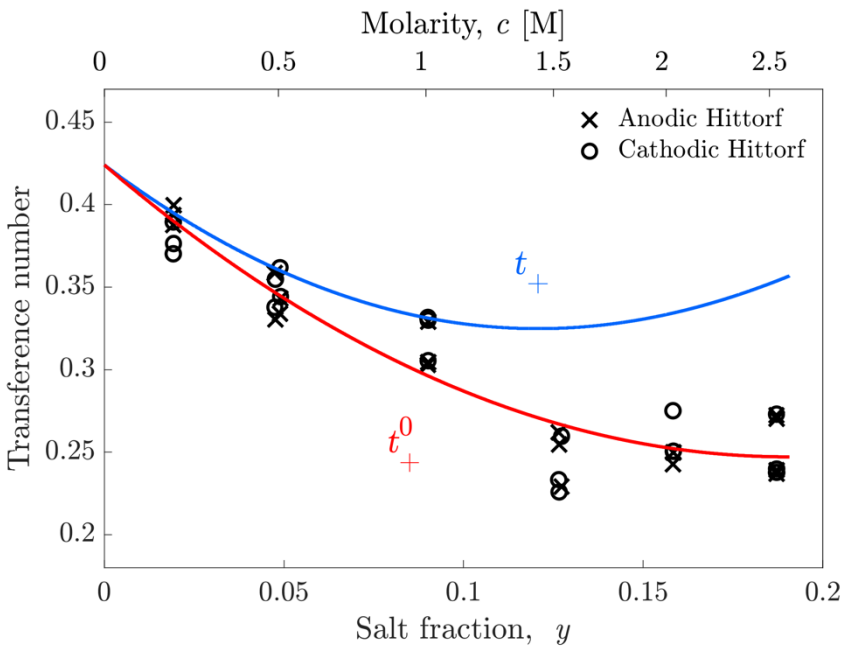

Figure 3. Hittorf measurements at 25 °C for the cation transference number t_+^0 of Li^+ relative to EMC, based on analysis of the anodic Hittorf chamber (x) and cathodic Hittorf chamber (o). The cation transference number (t_+^0) correlation from equation 11 (red —) is plotted alongside the cation transport number (t_+) from equation 12 (blue —).

3.3 Thermodynamic factor

Liquid-junction potentials measured at 25 °C with the shifting-reference concentration-cell method are shown in figure 4(a) for $LiPF_6$:EMC with reference concentrations ranging from y_{ref} = 0.0012-0.1678 (0.012 M-2.18 M) and figure 4(b) for $LiPF_6$:PC with references from y_{ref} = 0.0007-0.1436 (0.007 M-2.083 M). Primary data are tabulated in the supplementary information, tables S3 and S4. Each line in plots (a) and (b) represents a banded fit about each y_{ref} with the correlation

$$\Delta U(y) = U'_0(y - y_{ref}) + U'_1(y - y_{ref})^2 + U'_2\left[\ln\frac{y}{y_{ref}} + 1 - \frac{y}{y_{ref}}\right], \qquad (13)$$

arrived at by integrating equation 8 from y_{ref} to y. Fitting with the function from equation 13 is convenient for data analysis, because the fit parameter U'_0 directly produces the value of

$d\Delta U/dy|_{y_{\mathrm{ref}}}$ that appears in equation 7. Using the composition correlation for t_+^0 obtained from Hittorf experiments, one can also insert $t_+^0(y_{\mathrm{ref}})$ into this equation, allowing the thermodynamic factor $\chi(y_{\mathrm{ref}})$ to be isolated:

$$\chi(y_{\mathrm{ref}}) = \frac{1}{1 - t_+^0(y_{\mathrm{ref}})} \frac{F y_{\mathrm{ref}}}{\nu RT} U'_0|_{y_{\mathrm{ref}}}. \tag{14}$$

Results for χ obtained in this way are plotted for $LiPF_6$:EMC and $LiPF_6$:PC in figures 4(c) and 4(d), respectively.

The Debye–Hückel theory of ionicity suggests that the thermodynamic factors of strong electrolytes vary with the square root of composition [28]. Thus, correlations for $\chi(y)$ were determined by testing power series up to various orders in $\sqrt{y}$, optimizing to obtain tight parameter confidence intervals while maintaining goodness-of-fit. Correlations for χ_{EMC} and χ_{PC} based on this fitting approach are

$$\chi_{\mathrm{EMC}} = 1 - 18.38y^{1/2} + 155.3y - 465.6y^{3/2} + 1647y^{5/2}, \tag{15}$$

$$\chi_{\mathrm{PC}} = 1 - 2.655y^{1/2} + 26.23y + 1490y^{7/2}, \tag{16}$$

functions plotted on figure 4(c, d). Hou and Monroe [12] presented fixed-reference concentration-cell data for $LiPF_6$:PC ($y_{\mathrm{ref}} = 0.07648$). Figure 4(d) shows good agreement between the fixed-reference and shifting-reference approaches for $LiPF_6$:PC in the 0.2 M–2 M range where Hou and Monroe's correlation is valid for interpolation.

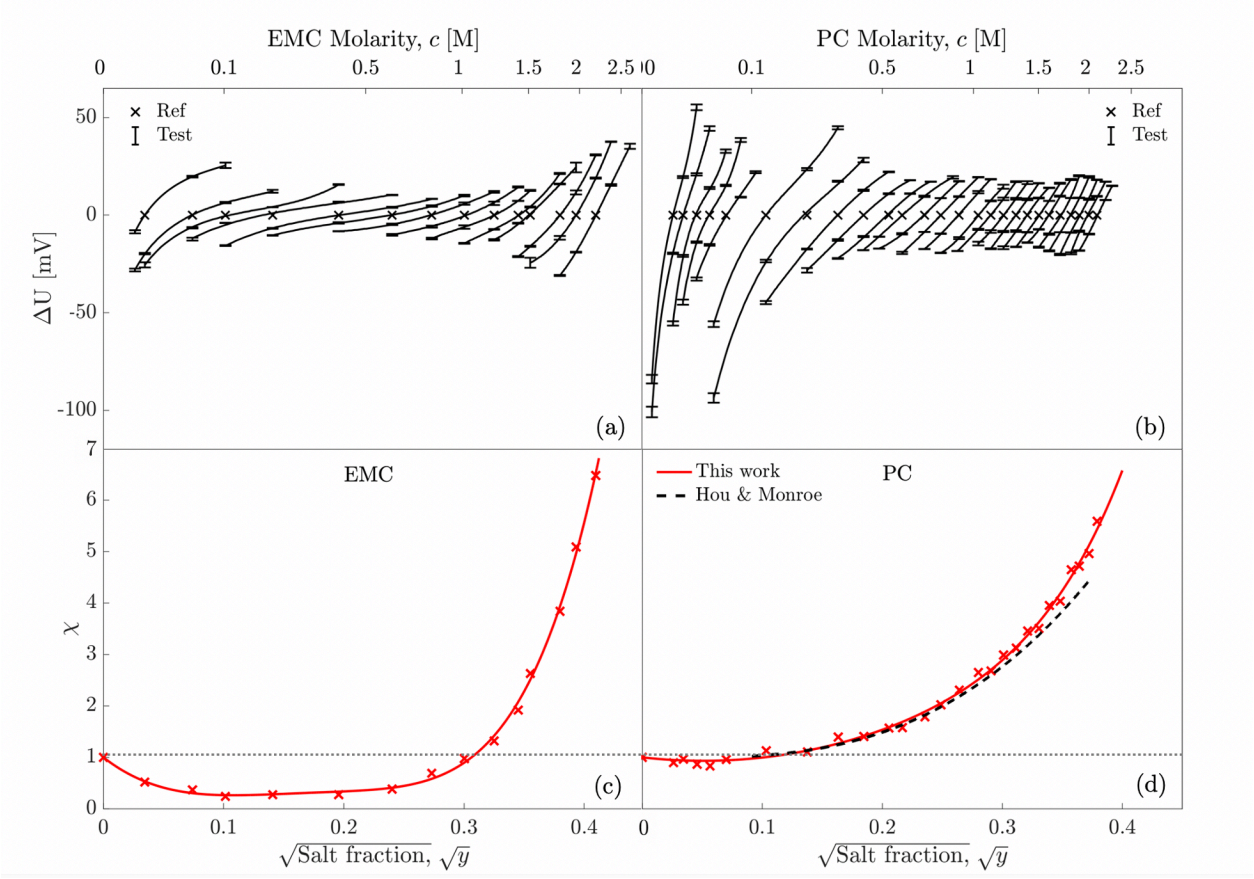

Figure 4. Banded liquid-junction potentials measured using the shifting-reference concentration-cell method for $LiPF_6$:EMC (a) and $LiPF_6$:PC (b). Error bars represent the standard deviation in the average of three replicate measurements and (x) indicate each reference composition $y_{ref.}$ Each band is fit by equation 13 (black —). Thermodynamic factor χ is plotted for $LiPF_6$:EMC (c) and $LiPF_6$:PC (d) at each y_{ref} (x) with correlations from equations 15 and 16 (red —), with $\chi = 1$ indicated by (gray ⋯). Panel (d) also shows the χ fitting from Hou and Monroe [12] using the fixed-reference method (black - - -).

At infinite dilution the thermodynamic factor χ for any dilute solute must go to unity, and the analysis of electrostatic interactions provided by Debye–Hückel theory [28] suggests that thermodynamic factors of electrolytes should fall with the square root of salt concentration when dilution is high. Although parameter ranges were not restricted during data fitting, the coefficients of the $\sqrt{y}$ terms in correlations 13 and 14, which we notate as $\chi_{\sqrt{y}}$ for brevity, were both naturally

negative. An implementation of Debye–Hückel theory following Newman and Thomas–Alyea [1] shows that $\chi_{\sqrt{y}}$ is expected to follow the limiting law

$$\chi_{\sqrt{y}} = -\frac{1}{8\pi N_{\mathrm{A}}}\sqrt{\frac{\rho_0}{2M_0}\left(\frac{F^2}{\varepsilon_{\mathrm{r}}\varepsilon_0 RT}\right)^3}, \tag{3}$$

in which N_{A} is Avogadro's number, ε_{r} is the relative permittivity of the solvent, and ε_0 is the permittivity of vacuum. Shifting-reference concentration-cell results remain consistent and achieve good signal-to-noise in the highly dilute regime, making them suitable to probe the validity of this relationship.

For $LiPF_6$:PC, Debye–Hückel theory predicts that $\chi_{\sqrt{y}}$ is –2.67, in good agreement with the value of –2.655 that appears in correlation 14. (NB: The fixed-reference concentration-cell data of Hou and Monroe for LiPF6:PC suggested a $\chi_{\sqrt{y}}$ value of –0.3243. They observed that this value was error-prone, however, because it required extrapolation of the χ correlation far outside their range of experimental test concentrations [12].)

For $LiPF_6$:EMC solutions, equation 17 predicts a much steeper theoretical Debye–Hückel slope: –250, far different from the value of –18.76 obtained from correlation 13. This discrepancy can be understood by recognizing that the Debye–Hückel analysis assumes that the concentrations of dissolved ions in solution arise from complete dissociation of the host salt – *i.e.*, it assumes that as well as measuring the salt content, *y* also measures the ionic strength [28]. If salt dissociation is incomplete, so that the extent of salt dissociation is some fraction $0 \leq \xi < 1$, then the slope will be lower in magnitude than the prediction of equation 17 by a factor of $\sqrt{\xi}$. The ratio of 18.38/250 = 0.074 suggests that the extent of dissociation for $LiPF_6$ in EMC is no more than 27% in the approach to infinite dilution – and could be much less.

Significant deviation of χ from the Debye–Hückel limiting law, as is observed for both $LiPF_6$:PC and $LiPF_6$:EMC at moderate concentrations, generally indicates that specific species/species interactions are causing non-ideal behavior that is not amenable to analysis with a classical electrostatic theory. Such chemical interactions can be interpreted qualitatively following the general principles laid out by Robinson and Stokes [2]. First, ion/ion interactions such as ion pairing and association serve to decrease the free energy of the solute in comparison to the solvent, hence decreasing the salt activity coefficient and, along with it, χ, which relates to the derivative of activity with respect to composition through equation 2. Second, ion/solvent interactions hold more solvent molecules in the solution phase, effectively decreasing the solvent's vapor pressure [29] and causing a corresponding increase in the solute's activity coefficient, leading to a consequent increase in χ. These competing trends are also substantiated by more recent electrolyte theories such as the binding mean spherical approximation [30]. Note that the crossing points where $\chi_{\mathrm{PC}} = 1$ at $\sqrt{y} \approx 0.1$ (0.12 M) and $\chi_{\mathrm{EMC}} = 1$ at $\sqrt{y} \approx 0.3$ (1.01 M) merely reflect compositions in which competing nonideal factors are in balance, rather than indicating thermodynamic ideality.

3.4 Conductivity, viscosity, and Stokes law model

Ionic conductivity κ trends through a maximum near 1.8 M for $LiPF_6$:EMC, as can be seen from the plot in figure S1 of the supplementary information. Experimental conductivity data are tabulated in table S5 of the supplementary information. Equivalent conductance Λ is plotted in figure 5; it is determined by dividing the ionic conductivity by the salt molarity, as well as the cation's charge and its stoichiometric coefficient in the neutral salt,

$$\Lambda = \frac{\kappa}{z_+ \nu_+ c}. \tag{18}$$

The hypothesis that dilute $LiPF_6$:EMC is a weak electrolyte is consistent with the nonlinear dependence of its equivalent conductance on $\sqrt{y}$ near infinite dilution, which contrasts the more typical response of a strong electrolyte exhibited by $LiPF_6$:PC. For data fitting of $LiPF_6$:EMC equivalent conductance, the functional form

$$\Lambda = \left(\Lambda_1 y^{1/4} + \Lambda_2 y^{1/2} + \Lambda_3 y^{5/4}\right)^2 \tag{19}$$

was chosen by systematically iterating through various functions of the form $\Lambda = [P_7(y^{1/4})]^2$, where $P_7(x)$ represents a 7th-order polynomial in x. An optimization algorithm was written to vary the number of nonzero coefficients in the polynomial, as well as the combination of powers associated with said coefficients, seeking the fit with the fewest parameters, highest R-squared value, and tightest confidence intervals. (More details are provided in the supplementary information.) All functions with fewer than 2 or more than 4 nonzero coefficients had higher error; the function in equation 19 had both the highest R-squared and tightest root-mean-squared average confidence intervals of all the 3-parameter fits. It is worth noting that when a constant term (nonzero coefficient of x^0) was included in P_7, the error was generally higher, and a null value of the constant was always within its confidence interval. Thus the fitting process does not confirm that the electrolyte reaches a finite equivalent conductance at infinite dilution, as Onsager–Fuoss theory would suggest [2]. Due to the qualitative nature of its development, it should be emphasized that correlation 19 is only strictly valid for interpolation, and should not be used outside the range of 0.05–2.15 M. Each parameter Λ_k is provided for temperatures 20, 25, and 30 °C in the correlation summary, Table 2.

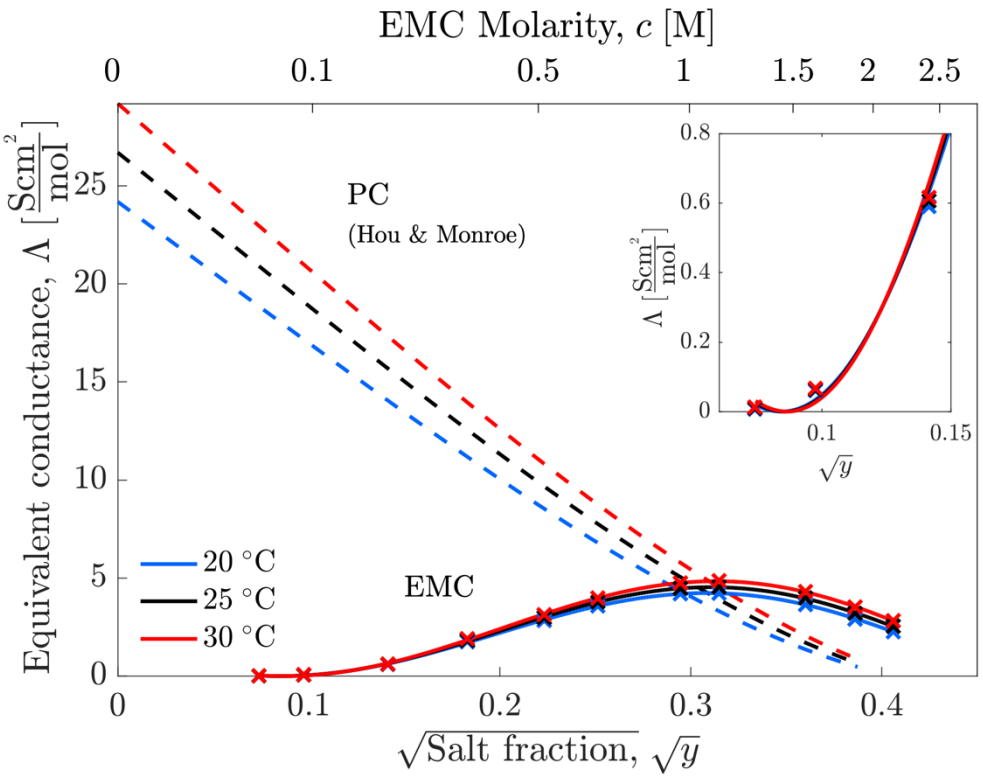

Figure 5. Equivalent conductances Λ at 20, 25, and 30 °C for $LiPF_6$:EMC (x) with (—) representing correlations based on fitting in equation 19 in the region valid for interpolation. Equivalent-conductance correlations for $LiPF_6$:PC from Hou and Monroe [12] are plotted for comparison (---).

Dynamic viscosity η was measured with respect to salt fraction y for both $LiPF_6$:EMC and $LiPF_6$:PC solutions. It generally increases with salt concentration, as shown in figure 6. Data were fit by a power series in $\sqrt{y}$, found using the error-minimization principles discussed earlier,

$$\eta = \eta_0 + \eta_1 y^{3/2} + \eta_2 y^{13/2}. \quad (20)$$

Each coefficient η_k is listed in table 2 for EMC and table 3 for PC, at temperatures of 20, 25, and 30 °C, and the raw data is tabulated in tables S6 and S7. $LiPF_6$:PC solutions were more viscous than $LiPF_6$:EMC at similar salt fractions across the range studied.

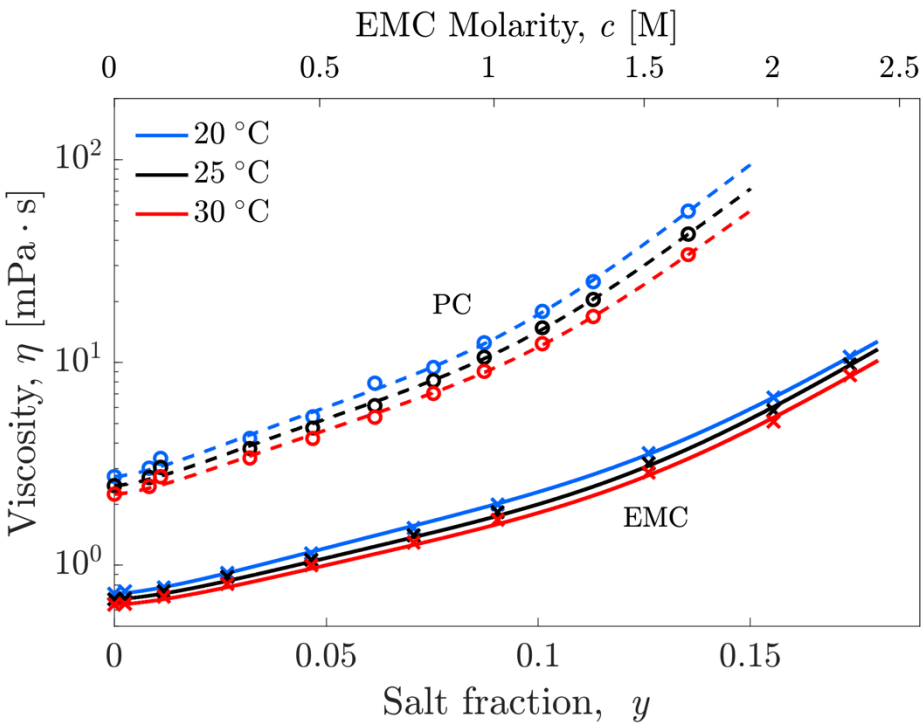

Figure 6. Dynamic viscosity η at 20, 25, and 30 °C for $LiPF_6$:EMC (x) and $LiPF_6$:PC (o), along with correlations at each temperature for $LiPF_6$:EMC (—) and $LiPF_6$:PC (---).

A Walden analysis using Stokes mobility relations can be applied to further elucidate differences in salt dissociation between the electrolytes studied. In very dilute solutions, the Stokes–Einstein relation suggests that the mobility u_i of solvated ion i in a homogenous background solvent relates to its hydrodynamic radius R_i through the solvent viscosity [31]. For mobile Li^+ cations,

$$u_+ = \frac{N_A}{6\pi\eta R_+}. \tag{21}$$

Nernst–Planck dilute-solution theory further suggests that equivalent conductance provides a measure of total ionic mobility, and that the transference number of a species measures its fractional contribution to this total. A cation equivalent conductance λ_+ can thus be defined by [1]

$$\lambda_+ = \Lambda t_+^0 = |z_+| F^2 u_+. \tag{22}$$

Walden's rule puts equations 21 and 22 together to draw the conclusion that the equivalent conductance should vary in direct proportion to the inverse viscosity ($\Lambda t_+^0 \propto 1/\eta$). The validity of this relationship is probed by the Walden plot in figure 7, which presents lithium equivalent conductance as a function of inverse viscosity – both of which are parametric functions of composition – for $LiPF_6$:EMC and $LiPF_6$:PC. The plot was created using the η correlations presented above for both solutions. Experimental correlations for Λ and t_+^0 of $LiPF_6$:EMC are also presented in Table 2; for $LiPF_6$:PC, these correlations were taken from Hou and Monroe [12].

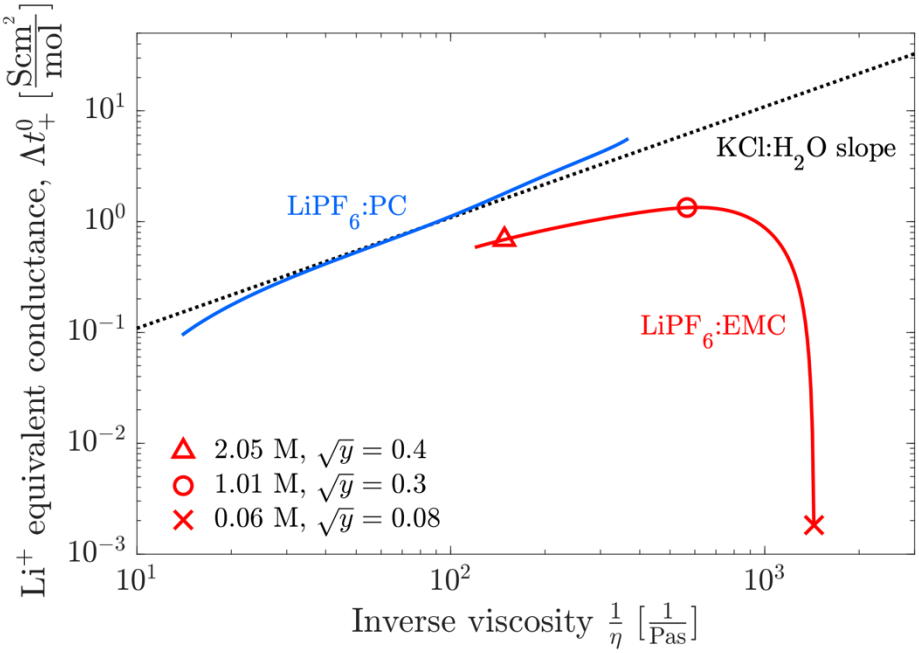

Figure 7. Walden analysis for cation equivalent conductance Λt_+^0 plotted against the inverse of viscosity $\frac{1}{\eta}$ at 25 °C for $LiPF_6$:EMC (red), and $LiPF_6$:PC (blue). Plot markers (△, o, x) serve to indicate composition trends while (…) represents the slope parallel to that of KCl in water to represent a well dissociated electrolyte [32].

The Stokes–Einstein relation assumes that ion/ion interactions do not affect their mobilities, and that the relative decrease in the solvent's volume fraction does not impact the ions' hydrodynamic radii. A comparison of the curves in figure 7 for $LiPF_6$:PC and $LiPF_6$:EMC with a

reference line parallel to the curve for KCl:H_2O — often taken as the standard in literature for a well-dissociated electrolyte [32] — suggests that $LiPF_6$ appears well dissociated in PC across the concentration range studied, while $LiPF_6$ in EMC does not at concentrations below 1.01 M. The inflection point at $\sqrt{y} = 0.3$ (c = 1.01 M) — indicated by the (o) marker for $LiPF_6$:EMC, above which the slope conforms better to Walden's rule — correlates well with the point in thermodynamic factor χ in figure 4(c) at $\sqrt{y} = 0.3$ where the thermodynamic effects of ion pairing balance solvation interactions ($\chi_{\mathrm{EMC}} \approx 1$). This observation highlights the important link between phenomenological transport properties and a solution's thermodynamic state. Further insight into microscopic species/species interactions may be gained by analyzing the Stefan–Maxwell drag coefficients between cation, anion, and solvent species.

3.5 Diffusion coefficient

Values of the effective Fickian diffusivity D_{eff} obtained from potentiometric restricted-diffusion experiments for $LiPF_6$:EMC are plotted in figure S3 and summarized in table S8 of the supplementary information. These were corrected to obtain Fickian diffusivities of the pure solution D via EIS measurements of inverse MacMullin numbers α, following the method of Hou and Monroe [12], who used the formula $D_{\mathrm{eff}}/D = \kappa_{\mathrm{eff}}/\kappa = \alpha$. This cell-specific MacMullin scaling of restricted-diffusion data helps resolve separator-to-separator variation, which arises in the present case from the highly variable tortuosity of randomly woven glass fiber. Although not used in the data processing for restricted diffusion, Bruggeman exponents b were calculated from experimental MacMullin-number measurements with the formula $\alpha = \varepsilon^b$ and the manufacturer's reported separator porosity $\varepsilon = 0.85$, yielding that $b = 1.23 \pm 0.74$. All the experimental MacMullin-number data are summarized in the supplementary information (figure S2).

Fickian diffusivity D for $LiPF_6$:EMC at 25 °C decreases across the concentration range and was fit with a second-order polynomial:

$$D = 504.8 \frac{\mu m^2}{s} \times (1 - 6.064y + 11.35y^2). \quad (4)$$

Figure 8 presents the composition dependence of Fickian diffusivity D as well as a thermodynamic diffusivity $\mathcal{D}$, based on a salt chemical-potential gradient driving force for diffusion, rather than a molarity gradient. The thermodynamic factor χ relates these through

$$D = \mathcal{D}\chi\,; \quad (24)$$

data on the plot were computed using equation 15. Ion association would be expected to increase the apparent thermodynamic diffusivity of the salt, because the merging of two or more species into a single particle implies a lower apparent resistance to the single particle's motion [2].

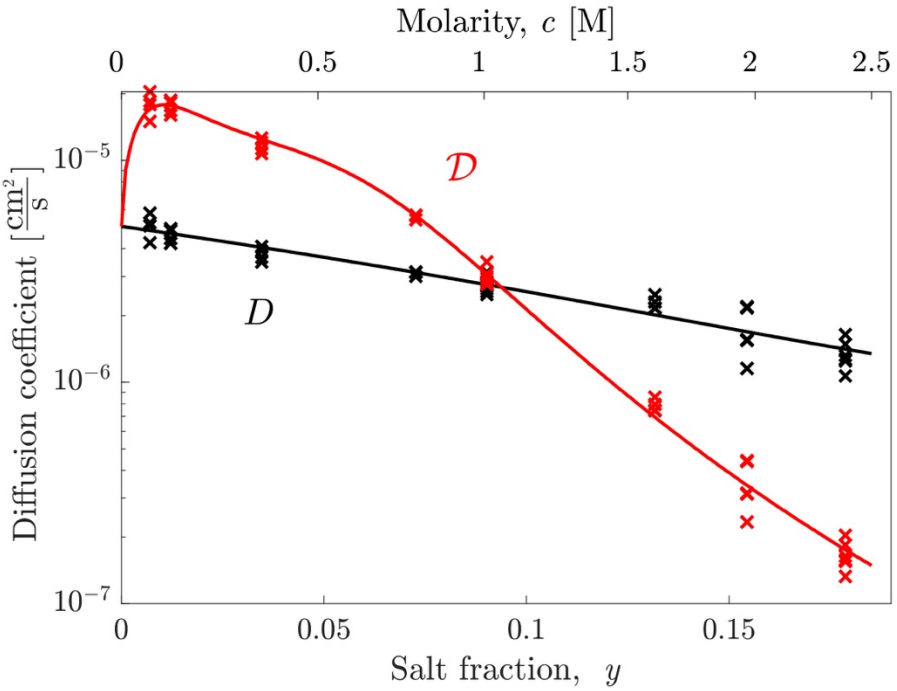

Figure 8. Fickian diffusion coefficient D (black) and thermodynamic diffusion coefficient $\mathcal{D}$ (red) of $LiPF_6$ in EMC at 25 °C. Curves show correlations that derive from equations 23 and 24.

3.6 Onsager–Stefan–Maxwell coefficients

The Onsager–Stefan–Maxwell formalism expresses transport laws in terms of thermodynamic forces that drive diffusion. Under isothermal, isobaric conditions, the balance between the thermodynamic force driving species *k* and the friction forces exerted on *k* by the relative motion of all other species is

$$-c_T y_k \vec{\nabla}\mu_k = RT \sum_{k \neq j} \frac{y_j \vec{N}_k - y_k \vec{N}_j}{D_{kj}}, \tag{25}$$

where $\vec{N}_k$ is the molar flux of species *k,* μ_k is its electrochemical potential*,* and y_k, its particle fraction; $\mathcal{D}_{kj}$ is the Stefan–Maxwell diffusivity of species *k* through species *j,* which may be interpreted as an inverse friction factor [1,12,15]. Transport models based on Onsager–Stefan–Maxwell theory incorporate microscopic species/species interactions, which can be significant in both concentrated electrolytes and weakly-dissociated dilute electrolytes. In a binary electrolytic solution, Stefan–Maxwell diffusivities can be directly computed from bulk transport properties through the mappings [1]

$$\mathcal{D}_{0-} = \frac{\nu_- \mathcal{D}}{\nu t_+^0}, \quad \mathcal{D}_{0+} = \frac{\nu_+ \mathcal{D}}{\nu(1-t_+^0)}, \qquad \frac{1}{\mathcal{D}_\pm} = \frac{F^2 z_+}{RT\nu_- \Lambda y} - \frac{\nu(1-\nu y)t_+^0(1-t_+^0)}{\nu_+ \nu_- \mathcal{D} y}. \tag{26}$$

Note that when analyzing the binary $LiPF_6$:EMC electrolytes studied here, the individual species were taken to be the cation Li^+ (+), anion PF_6^- (–), and solvent EMC (0), and *y* was consequently computed assuming complete dissociation of the salt. As first pointed out by Onsager [24], this possible misidentification of species' states in a weak electrolytic solution will not affect the number of independent parameters in a thermodynamic model so long as the number of independently variable species concentrations assigned to the system is correct. Thus the assumption that an electrolyte is strong when defining and computing its properties does not have an effect if it exists in a dissociation equilibrium. Within a multicomponent transport model, the

same observation holds true so long as local association/dissociation equilibrium is achieved with very rapid kinetics compared to the characteristic timescales associated with transport phenomena.

It is worth noting that the explicit consideration of associated $[(\mathrm{Li})_x(\mathrm{PF_6})_y(\mathrm{solvent})_z]^{x-y}$ complexes as additional species, both within the system's equilibrium constitutive formulation and the transport constitutive laws, could permit a more detailed understanding of how the phenomenological material properties depend on composition. Under the assumption that the kinetics of every speciation reaction is fast, both $\mathrm{LiPF_6}$:PC and $\mathrm{LiPF_6}$:EMC are treated here as 'pseudo-binary' electrolytic solutions, which can be described completely by a three-species transport model. Explicit accounting for ion pairs has been attempted recently using simulations based on Nernst–Planck–Poisson transport equations [33], but that constitutive framework neglects solute/solute interactions and does not explicitly couple the species electrochemical potentials through reaction equilibria. A similar extension of the present theory is possible, but would introduce many unknown parameters into both the thermodynamic model and the Onsager–Stefan–Maxwell formulation, as well as complicating the theoretical relationships among macroscopic and microscopic parameters (*cf.* equation 26). For example, the consideration of a single additional dissolved species – say, undissociated salt, as well as dissociated cations and anions – would introduce two additional thermodynamic factors and a new partial molar volume, as well as three additional Stefan–Maxwell diffusivities, into the parameter space of the model. An explicit accounting for ion-association effects will therefore be left to a future, more theoretical analysis, which may also shed light on the macroscopic impacts of slow speciation kinetics.

Figure 9 shows the Stefan–Maxwell coefficients for $\mathrm{LiPF_6}$:EMC solutions, calculated using the transport-property correlations at 25 °C summarized in table 2. The relatively low value of the ion/ion diffusivity $\mathcal{D}_{+-}$, being up to five orders of magnitude lower than the solvent/ion

Stefan–Maxwell coefficients at high dilution, suggests substantial ion pairing. This observation is consistent with both the Robinson–Stokes perspective on thermodynamic factor and the Walden analysis of cation equivalent conductance. As $LiPF_6$ content increases, $\mathcal{D}_{0-}$ and $\mathcal{D}_{0+}$ decrease by two orders of magnitude, as the solvent exerts stronger drag on solvated cations and anions; the fall is steeper at compositions where $\chi_{\mathrm{EMC}} > 1$ in figure 4(c). Unlike the $\mathcal{D}_{+-}$ values measured for $LiPF_6$ in PC by Hou and Monroe [12], $\mathcal{D}_{+-}$ for $LiPF_6$ in EMC increases across the concentration range, and does not pass through a maximum at the same composition as ionic conductivity does. This suggests that the effects of cation/anion coordination due to a lack of free solvent are not important for this electrolyte below 2 M.

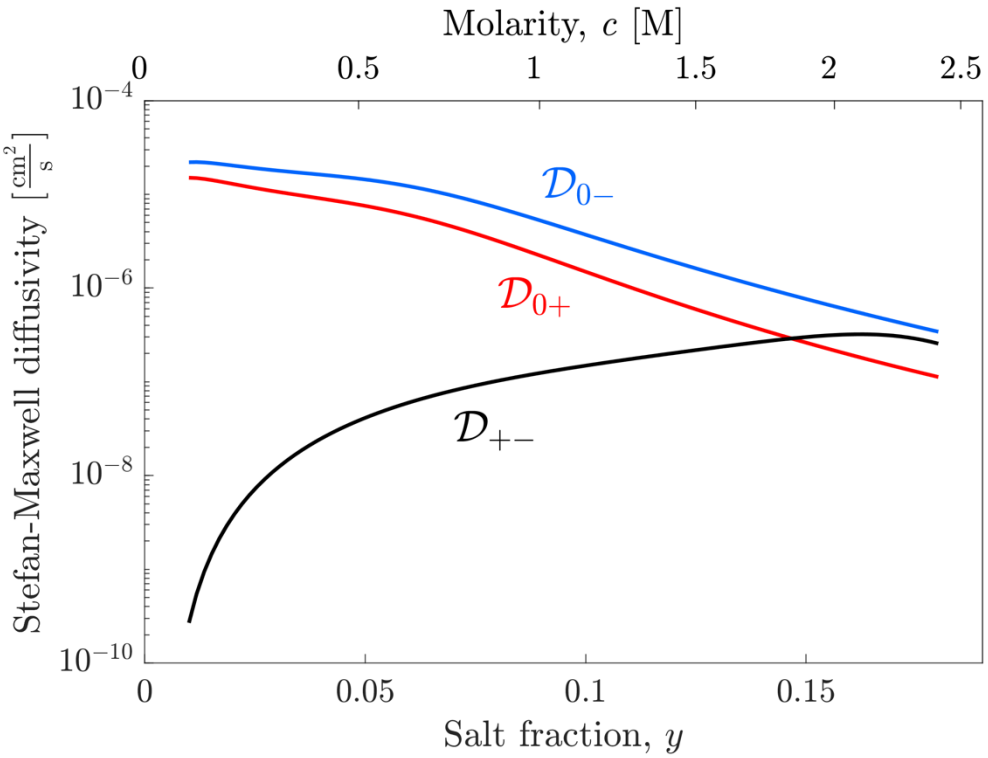

Figure 9. Stefan–Maxwell coefficients for $LiPF_6$:EMC at 25 °C calculated from property correlations in the composition ranges valid for interpolation.

3.7 On ion association

Results from sections 3.3, 3.4, and 3.6 for $LiPF_6$ salt in EMC and PC are better understood by comparing the physicochemical properties of EMC and PC associated with solvation, which are presented in table 1. Pure PC has a much higher relative permittivity and polarity (dipole moment) compared to pure EMC. Ion pairing has been demonstrated to depend on solvent donicity and Lewis-base characteristics [34,35], but a purely electrostatic perspective on solvation suffices to rationalize how higher-polarity PC molecules should stabilize isolated ions more than EMC. The electrostatic (Born) free energy of solvation $-\Delta G_{\mathrm{el}}$ is less exergonic for EMC, as it scales with $1-\frac{1}{\varepsilon_{\mathrm{r}}}$ [2]. Finally, in the Bjerrum theory [36], two opposing ions may be considered associated if they are separated by less than the Bjerrum critical distance [22], indicating that Li^+ and PF_6^- must be much closer together in PC for electrostatic interactions to favor ion pairing [2].

Table 1. Relative permittivity ε_{r}, dipole moment, and calculated Bjerrum critical distance q for EMC and PC solvents at 25 °C [37].

Solvent	ε_{r}	dipole moment (D)	q (nm)
EMC	2.958	0.89	9.474
PC	64.92	4.81	0.431

The suppressed thermodynamic factor χ revealed by shifting-reference concentration-cell measurements, non-linear Walden plot, and low ion/ion Stefan–Maxwell diffusivity all corroborate the hypothesis that the extent of dissociation is low for dilute $LiPF_6$ in EMC, contrasting $LiPF_6$:PC, in which no significant ion-pairing effects are seen below 0.5 M.

It is worth emphasizing that ion pairing has consequences for measured thermodynamic properties as well as ion-transport mechanisms. The interpretation of spectroscopic data for ion association often relies on observations of relative changes in absorption spectra and bond

symmetry; hence the thermodynamic and transport markers of ion pairing provide additional context when absorption spectra for solvent and solute molecules overlap [38]. In addition, the comparison between $LiPF_6$:EMC and $LiPF_6$:PC properties above supports the preferential-solvation narrative for cyclic carbonate solvents over acyclic carbonates in conventional commercial Li-ion electrolytes [39,40]. Even minor addition of a strongly-solvating cyclic carbonate such as PC or ethylene carbonate to $LiPF_6$ in a linear carbonate such as EMC causes the electrolyte's properties to adhere disproportionately to those associated with cyclic-carbonate solvation [6,38,41,42]. Future multicomponent transport models based on Onsager–Stefan–Maxwell concentrated-solution theory for co-solvent systems may yield further insights when combined with spectroscopy and compared against the data presented for binary electrolytes in this work.

Yet for electrolytic solutions wherein ion speciation or association is locally quasi-equilibrated on the timescales relevant to bulk transport, the distinction between free ions and associated pairs may not be important for continuum-level electrolyte models. A consistent composition basis and a complete thermodynamic and transport parametrization allows for the accurate simulation of dynamical electrolyte behavior regardless of degree of dissociation, as shown by Hou & Monroe for $LiPF_6$:PC [12] and in section 3.7 and appendix A2 below for $LiPF_6$:EMC.

3.7 Parameter summary and validation

Table 2 provides a summary of the property correlations discussed throughout this work. Please note that composition bases may be easily interchanged between salt fraction y, molarity c, and mass fraction ω by applying equations 3 and 4.

The full transport and thermodynamic property characterization of $LiPF_6$:EMC presented here allows the implementation of the electrolyte transport models put forward by Hou, Liu, and

Monroe [12,15,18], which are based on an extended concentrated-solution theory that includes solute-volume effects. The measured voltage drop across the electrolyte relates to changes in cation electrochemical potential, which are dictated in part by the composition dependence of the thermodynamic factor χ. Figure A2 of the Appendix shows good agreement between experimental and simulated results of restricted-diffusion voltage relaxations at 25 °C, validating the parameter correlations presented here for $LiPF_6$:EMC solutions.

Table 2. Summary of parameter correlations for properties measured in this work. Note the composition basis is salt fraction y for all correlations except density ρ where molarity is used to easily calculate partial molar volumes discussed in appendix A1. Remaining $LiPF_6$:PC correlations are available in reference [12]. Constants in these functions are reported to 3 or 4 significant figures to ensure smooth fits; measurements of parameter uncertainties (95% confidence intervals) are reported in supplementary table S9.

Electrolyte	Property	T / °C	Correlation	Units
$LiPF_6$:EMC	$\rho(c\ [M])$	20	$1013.1 + 113.19c - 7.8842c^{3/2}$	gL^{-1}
		25	$1007.1 + 114.20c - 8.1212c^{3/2}$	gL^{-1}
		30	$1001.1 + 115.13c - 8.3005c^{3/2}$	gL^{-1}
	$\eta(y)$	20	$0.724 + 43.80y^{3/2} + 5.964 \times 10^5 y^{13/2}$	mPa·s
		25	$0.680 + 36.01y^{3/2} + 5.655 \times 10^5 y^{13/2}$	mPa·s
		30	$0.639 + 32.17y^{3/2} + 4.917 \times 10^5 y^{13/2}$	mPa·s
	$\Lambda(y)$	20	$\left(-9.273y^{1/4} + 33.39y^{1/2} - 58.50y^{5/4}\right)^2$	Scm^2mol^{-1}
		25	$\left(-9.631y^{1/4} + 34.46y^{1/2} - 59.64y^{5/4}\right)^2$	Scm^2mol^{-1}
		30	$\left(-9.970y^{1/4} + 35.47y^{1/2} - 60.66y^{5/4}\right)^2$	Scm^2mol^{-1}
	$\chi_{EMC}(y)$	25	$1 - 18.38y^{1/2} + 155.3y - 465.6y^{3/2} + 1647y^{5/2}$	—
	$t_+^0(y)$	25	$0.4240 - 1.858y + 4.880y^2$	—
	$D(y)$	25	$504.8(1 - 6.064y + 11.35y^2)$	$\mu m^2 s^{-1}$
$LiPF_6$:PC	$\eta(y)$	20	$2.74 + 287.9y^{3/2} + 1.702 \times 10^7 y^{13/2}$	mPa·s
		25	$2.47 + 246.7y^{3/2} + 1.245 \times 10^7 y^{13/2}$	mPa·s
		30	$2.24 + 212.3y^{3/2} + 9.382 \times 10^6 y^{13/2}$	mPa·s
	$\chi_{PC}(y)$	25	$1 - 2.655y^{1/2} + 26.23y + 1490y^{7/2}$	—

4. Conclusion

An improvement to the experimental methodology for concentration-cell measurements was implemented by using a shifting reference concentration, which creates a banded surface of liquid-junction potentials that can be fit to interpolate how the potential changes with composition. The method was demonstrated and combined with Hittorf transference-number measurements and densitometry data to quantify composition-dependent thermodynamic factors χ for $LiPF_6$ in EMC and $LiPF_6$ in PC up to approximately 2 M concentrations. The shifting-reference concentration-cell method reduces error in the liquid-junction potential resulting from proportionally large concentration differences and the composition dependence of the cation transference number. This combination of techniques can be applied to new electrolyte formulations to assess their departures from thermodynamic ideality, which in turn governs the concentration overpotentials expected in full-cell configurations operated at higher power. Conductivity and viscosity measurements were used to implement a Walden analysis that showed the mobility of lithium of $LiPF_6$:EMC to differ substantially from expectations based on the Stokes–Einstein relation. Finally, a full set of macroscopic transport properties: transference number, equivalent conductance, and thermodynamic diffusivity, was mapped into Stefan–Maxwell coefficients that describe the microscopic species/species interactions in $LiPF_6$:EMC.

All three of these approaches demonstrate the impact of ion pairing, manifested in the suppression of thermodynamic factor χ, askew Walden plot, and extremely high cation/anion friction factors in the dilute regime which were apparent in weakly-dissociated $LiPF_6$:EMC, but not in strongly-dissociated $LiPF_6$:PC.

Agreement between simulation and experiment for both weak and strong binary electrolytes suggests that the weakness of the $LiPF_6$:EMC electrolyte does not affect the accuracy

of transport models rooted in concentrated-solution theory based on an Onsager–Stefan–Maxwell formalism that accounts for three independent species. Further spectroscopic measurements, as well as measurements across wider temperature ranges, could provide additional information about association/dissociation equilibrium and kinetics in the future.

Acknowledgements

This work was supported by the Faraday Institution Multiscale Modelling Project, subaward FIRG003 under EPSRC grant number EP/S003053/1.

Appendix A1 – Partial Molar Volumes

Partial molar volumes of salt $\overline{V}_{\mathrm{e}}$ and solvent $\overline{V}_0$ describe how volume is distributed across the species in a binary electrolytic solution. They are critical for quantifying solute-volume effects such as Faradaic convection and the excluded-volume effect, which are transport mechanisms distinct from diffusion, migration, and convection, and are explicitly incorporated in the polarization-cell models used for simulations in this work [15]. For a binary electrolyte, partial molar volumes can be derived from density/molarity correlations through [1]

$$\overline{V}_{\mathrm{e}} = \frac{M_{\mathrm{e}} - \frac{d\rho}{dc}}{\rho - c\frac{d\rho}{dc}} \quad \text{and} \quad \overline{V}_0 = \frac{M_0}{\rho - c\frac{d\rho}{dc}}. \tag{A1}$$

Figure A1 presents the partial molar volumes for $LiPF_6$:EMC solutions derived from the correlation in equation 10.

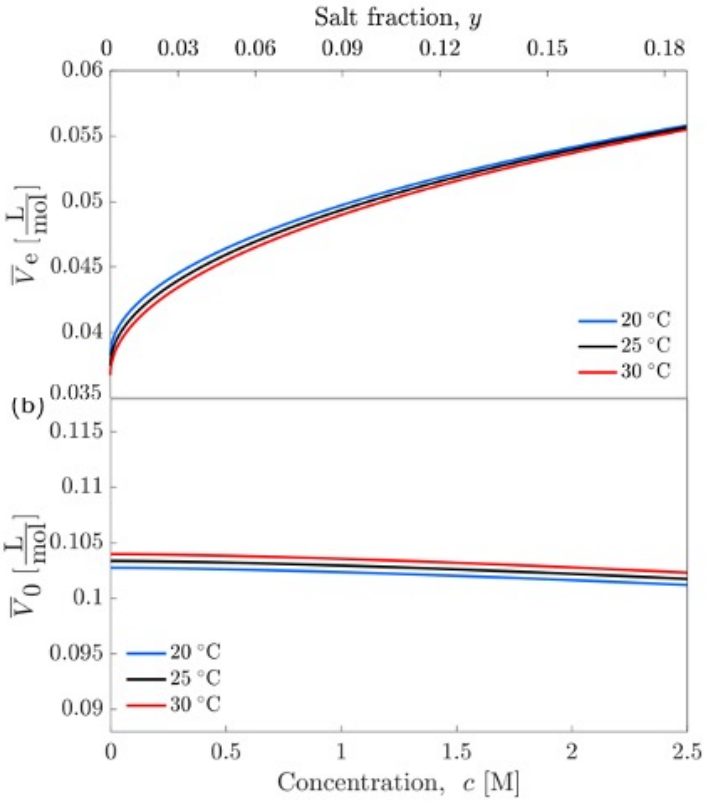

Figure A1 (a) Partial molar volume of solute $\overline{V}_e$, and (b) partial molar volume of solvent $\overline{V}_0$ as a function of $LiPF_6$ molarity in EMC at 20, 25, and 30 °C.

Appendix A2 – Validation of property correlations for $LiPF_6$:EMC

Parameters tabulated in table 2 were incorporated into a polarization-cell model to simulate restricted diffusion, as implemented by Hou and Monroe for $LiPF_6$:PC with COMSOL multiphysics software [12]. Restricted-diffusion measurements on cells constructed following the method outlined in section 2.7 at 25 °C were performed in triplicate at each $LiPF_6$ concentration, with an applied constant-current pulse at 0.199 mA/cm^2 for a duration of 12 hours. Data from the cells that were simulated, along with the transient measure of the residual error in mV, are presented in Figure A2. These cells were excluded from the parameterization process.

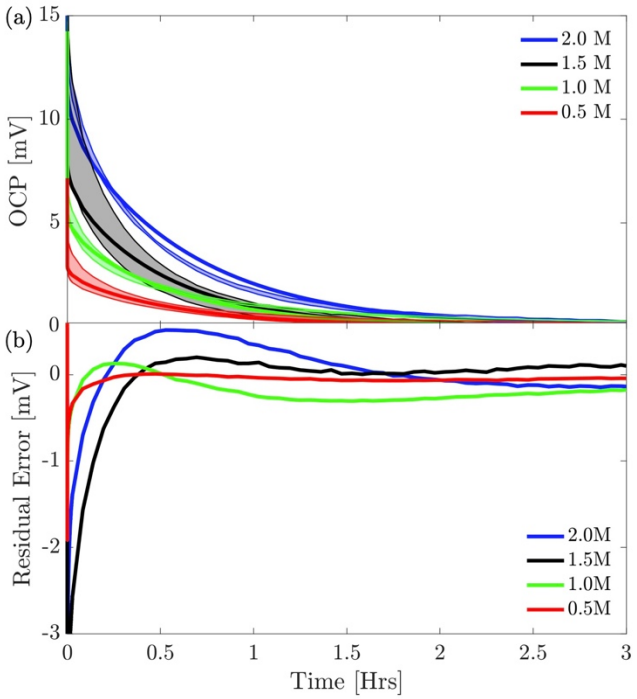

Figure A2 (a) Comparison between simulated results (solid —) and an average of three restricted-diffusion experiments with standard deviation in relaxation profiles plotted as the shaded region for four concentrations of $LiPF_6$:EMC. (b) Mean of residual errors between experiment and simulated results.

Appendix A3 – Supplementary information

Supplementary data to this article can be found online at:

List of symbols

Abbreviations

EIS	Electrochemical impedance spectroscopy
EMC	Ethyl methyl carbonate
OCP	Open-circuit potential
PC	Propylene carbonate
PEEK	Polyether ether ketone
PTFE	Polytetrafluoroethylene

Roman

A	Cross-sectional area, see supplementary information. [cm^2]
b	Bruggeman exponent, see supplementary information. [unitless]
c	Molar salt concentration. [M = mol/L]
c_-	Anion molarity; $c_- = \nu_- c$. [M = mol/L]
c_+	Cation molarity; $c_+ = \nu_+ c$. [M = mol/L]
c_0	Solvent molarity; $c_0 \overline{V}_0 = 1 - \overline{V}_e c$. [M = mol/L]
c_T	Total particle molarity, $c_T = c_0 + c_- + c_+$. [M = mol/L]
c_f	Salt concentration at end of Hittorf experiment. [M = mol/L]

1	D	Fickian diffusivity. [cm^2s^{-1}]
2	D_{eff}	Effective Fickian diffusivity in a solution-permeated separator. [cm^2s^{-1}]
3	$\mathcal{D}$	Thermodynamic diffusivity, see eq. 22. [cm^2s^{-1}]
4	$\mathcal{D}_{ij}$	Stefan–Maxwell diffusivity of species *i* in *j*. [cm^2s^{-1}]
5	F	Faraday's constant, 96485 $Cmol^{-1}$
6	$f_{\pm}$	Mean molar activity coefficient over molar basis.
7	ΔG_{el}	Electrostatic Gibbs free energy of solvation. [J]
8	I_{pulse}	Constant current applied to Hittorf cell. [A]
9	L	Cell or chamber length. [cm]
10	M_{e}	Molar mass of salt. [$gmol^{-1}$]
11	M_0	Molar mass of solvent. [$gmol^{-1}$]
12	N_{A}	Avogadro's number, 6.0221×10^{23} mol^{-1}
13	$\vec{N}_j$	Total molar flux of species *j*. [$molm^{-2}s^{-1}$]
14	q	Bjerrum critical distance. [m]
15	R	Gas constant, 8.3145 $Jmol^{-1}K^{-1}$
16	R_+	Stokes solvated radius of cation. [m]
17	t	Time during restricted diffusion relaxation. [s]
18	t_+	Cation transport number, see eq. 10. [unitless]
19	t_+^0	Cation transference number relative to the solvent velocity. [unitless]
20	T	Absolute temperature. [K]
21	T_{pulse}	Duration of constant current applied to Hittorf cell. [s]
22	ΔU	Steady-state liquid-junction potential of concentration cell. [V]
23	u_+	Cation mobility. [$m^2s^{-1}V^{-1}$]
24	$\overline{V_{\mathrm{e}}}$	Partial molar volume of salt. [$Lmol^{-1}$]
25	$\overline{V_0}$	Partial molar volume of solvent. [$Lmol^{-1}$]
26	V_{chamber}	Chamber volume in Hittorf cell. [L]
27	y	Salt particle fraction, see eq. 2. [unitless]
28	y_0	Solvent particle fraction.
29	y_{ref}	Reference composition in concentration cell. [unitless]
30	y_{test}	Test composition in concentration cell. [unitless]
31	z_-	Anion equivalent charge. [unitless]
32	z_+	Cation equivalent charge. [unitless]
33		
34	*Greek*	
35	α	MacMullin number, see supplementary information eq. S2. [unitless]
36	$\gamma_{\pm}$	Mean molar activity coefficient over molal basis.
37	ε	Separator porosity. [unitless]
38	ε_{r}	Relative permittivity of solvent. [unitless]
39	ε_0	Dielectric permittivity of vacuum. [unitless]
40	η	Dynamic viscosity. [mPas]
41	κ	Ionic conductivity. [$Scm^{-1}M^{-1}$]
42	κ_{eff}	Effective ionic conductivity in a solution-permeated separator. [$mScm^{-1}$]
43	Λ	Equivalent conductance. [Scm^2mol^{-1}]
44	λ_+	Cation equivalent conductance. [Scm^2mol^{-1}]
45	$\lambda_{\pm}$	Mean molar activity coefficient over particle-fraction basis.

μ_k	Electrochemical potential of species k. [Jmol^{-1}]
ν_-	Anion stoichiometry in a salt formula unit. [unitless]
ν_+	Cation stoichiometry in a salt formula unit. [unitless]
ν	Total number of ions in a salt formula unit, $\nu = \nu_+ + \nu_-$. [unitless]
ξ	Extent of dissociation. [unitless]
ρ	Mass density of solution. [gL^{-1}]
χ	Thermodynamic factor. [unitless]
ω	Salt mass fraction in solution. [unitless]
Ω_{bulk}	Bulk impedance measured with EIS, see supplementary information eq. S1. [Ω]

References

[1] Newman J, Thomas-Alyea KE. Electrochemical Systems. 3rd, illustr ed. John Wiley & Sons, 2004; 2004.

[2] Robinson RA, Stokes RH. Electrolyte Solutions: Second Revised Edition. 2nd ed. Dover Publications, Incorporated; 2012.

[3] Pitzer KS. Activity Coefficients in Electrolyte Solutions. 2nd Editio. 1991. https://doi.org/10.1201/9781351069472.

[4] Stewart S, Newman J. Measuring the Salt Activity Coefficient in Lithium-Battery Electrolytes. J Electrochem Soc 2008;155:A458. https://doi.org/10.1149/1.2904526.

[5] Valoen LO, Reimers JN. Transport Properties of LiPF6-Based Li-Ion Battery Electrolytes. J Electrochem Soc 2005;152:A882. https://doi.org/10.1149/1.1872737.

[6] Lundgren H, Behm M, Lindbergh G. Electrochemical Characterization and Temperature Dependency of Mass-Transport Properties of LiPF6 in EC:DEC. J Electrochem Soc 2014;162:A413–20. https://doi.org/10.1149/2.0641503jes.

[7] Nyman A, Behm M, Lindbergh G. Electrochemical characterisation and modelling of the mass transport phenomena in LiPF6-EC-EMC electrolyte. Electrochim Acta 2008;53:6356–65. https://doi.org/10.1016/j.electacta.2008.04.023.

[8] Lundgren H, Scheers J, Behm M, Lindbergh G. Characterization of the Mass-Transport Phenomena in a Superconcentrated LiTFSI:Acetonitrile Electrolyte. J Electrochem Soc 2015;162:A1334–40. https://doi.org/10.1149/2.0961507jes.

[9] Shah DB, Nguyen HQ, Grundy LS, Olson KR, Mecham SJ, Desimone JM, et al. Difference between approximate and rigorously measured transference numbers in fluorinated electrolytes. Phys Chem Chem Phys 2019;21:7857–66. https://doi.org/10.1039/c9cp00216b.

[10] Galluzzo MD, Loo WS, Wang AA, Walton A, Maslyn JA, Balsara NP. Measurement of Three Transport Coefficients and the Thermodynamic Factor in Block Copolymer Electrolytes with Different Morphologies 2020. https://doi.org/10.1021/acs.jpcb.9b11066.

[11] Ma Y, Doyle M, Fuller TF, Doeff MM, De Jonghe LC, Newman J. The Measurement of a Complete Set of Transport Properties for a Concentrated Solid Polymer Electrolyte Solution. J Electrochem Soc 1995;142:1859–68. https://doi.org/10.1149/1.2044206.

[12] Hou T, Monroe CW. Composition-dependent thermodynamic and mass-transport characterization of lithium hexafluorophosphate in propylene carbonate. Electrochim Acta 2019:135085. https://doi.org/10.1016/j.electacta.2019.135085.

[13] Craig N, Mullin SA, Pratt R, Crane GB. Determination of Transference Number and Thermodynamic Factor by use of Anion-Exchange Concentration Cells and Concentration Cells. J Electrochem Soc 2019;166:A2769–75. https://doi.org/10.1149/2.0351913jes.

[14] Pesko DM, Timachova K, Bhattacharya R, Smith MC, Villaluenga I, Newman J, et al. Negative Transference Numbers in Poly(ethylene oxide)-Based Electrolytes. J Electrochem Soc 2017;164:E3569–75. https://doi.org/10.1149/2.0581711jes.
[15] Liu J, Monroe CW. Solute-volume effects in electrolyte transport. Electrochim Acta 2014;135:447–60. https://doi.org/10.1016/j.electacta.2014.05.009.
[16] Darken LS. Diffusion, mobility and their interrelation through free energy in binary metallic systems. Trans Am Inst Min Metall Eng 1948;175:184–201. https://doi.org/10.1007/s11661-010-0177-7.
[17] Guggenheim EA. Thermodynamics. An Advanced Treatment for Chemists and Physicists. vol. 5. 5th ed. North-Holland Publishing Company, Amsterdam; 2019. https://doi.org/10.1515/zna-1950-0413.
[18] Liu J, Monroe CW. On the characterization of battery electrolytes with polarization cells. Electrochim Acta 2015;167:357–63. https://doi.org/10.1016/j.electacta.2015.03.104.
[19] Suo L, Hu YS, Li H, Armand M, Chen L. A new class of Solvent-in-Salt electrolyte for high-energy rechargeable metallic lithium batteries. Nat Commun 2013;4:1–9. https://doi.org/10.1038/ncomms2513.
[20] Thompson SD, Newman J. Differential Diffusion Coefficients of Sodium Polysulfide Melts. J Electrochem Soc 1989;136:3362. https://doi.org/10.1149/1.2096451.
[21] Gunnarshaug AF, Kjelstrup S, Bedeaux D, Richter F, Burheim OS. The reversible heat effects at lithium iron phosphate- and graphite electrodes. Electrochim Acta 2020;337. https://doi.org/10.1016/j.electacta.2019.135567.
[22] Marcus Y, Hefter G. Ion pairing. Chem Rev 2006;106:4585–621. https://doi.org/10.1021/cr040087x.
[23] Fong KD, Self J, Diederichsen KM, Wood BM, McCloskey BD, Persson KA. Ion Transport and the True Transference Number in Nonaqueous Polyelectrolyte Solutions for Lithium Ion Batteries. ACS Cent Sci 2019;5:1250–60. https://doi.org/10.1021/acscentsci.9b00406.
[24] Hemmer PC, Holden H, Ratkje SK. The Collected Works of Lars Onsager. World Scientific; 1996. https://doi.org/https://doi.org/10.1142/3027.
[25] Mindemark J, Lacey MJ, Bowden T, Brandell D. Beyond PEO—Alternative host materials for Li+-conducting solid polymer electrolytes. Prog Polym Sci 2018;81:114–43. https://doi.org/10.1016/j.progpolymsci.2017.12.004.
[26] Evans J, Vincent CA, Bruce PG. Electrochemical measurement of transference numbers in polymer electrolytes. Polymer (Guildf) 1987;28:2324–8. https://doi.org/10.1016/0032-3861(87)90394-6.
[27] Fuller TF, Doyle M, Newman J. Simulation and Optimization of the Dual Lithium Ion Insertion Cell. J Electrochem Soc 1994;141:1. https://doi.org/10.1149/1.2054684.
[28] Debye PJW. Collected papers of Peter JW Debye. Interscience Publishers; 1954.
[29] Pitzer KL. Activity coefficients in electrolyte solutions and molten salts. vol. 2. 2002. https://doi.org/10.1016/s1288-3255(00)87690-x.
[30] Crothers AR, Radke CJ, Prausnitz JM. 110th Anniversary : Theory of Activity Coefficients for Lithium Salts in Aqueous and Nonaqueous Solvents and in Solvent Mixtures . Ind Eng Chem Res 2019;58:18367–77. https://doi.org/10.1021/acs.iecr.9b02657.
[31] Stokes GG. Mathematical and Physical Papers. Cambridge Univ Press 1880. https://doi.org/10.1017/cbo9780511702297.
[32] Schreiner C, Zugmann S, Hartl R, Gores HJ. Fractional walden rule for ionic liquids: Examples from recent measurements and a critique of the so-called ideal KCl line for the

walden plot. J Chem Eng Data 2010;55:1784–8. https://doi.org/10.1021/je900878j.
[33] Richardson G, Foster JM, Sethurajan AK, Krachkovskiy SA, Halalay IC, Goward GR, et al. The effect of ionic aggregates on the transport of charged species in lithium electrolyte solutions. J Electrochem Soc 2018;165:H561–7. https://doi.org/10.1149/2.0981809jes.
[34] Matsubara K, Kaneuchi R, Maekita N. 13C NMR estimation of preferential solvation of lithium ions in non-aqueous mixed solvents. J Chem Soc - Faraday Trans 1998;94:3601–5. https://doi.org/10.1039/a807010e.
[35] Marcus Y. The effectivity of solvents as electron pair donors. J Solution Chem 1984;13:599–624. https://doi.org/10.1007/BF00650369.
[36] Bjerrum NJ. INVESTIGATIONS ABOUT ION ASSOCIATION. I. Dan Vidensk Selsk 1926;7:9.
[37] Xu K. Nonaqueous liquid electrolytes for lithium-based rechargeable batteries. Chem Rev 2004;104:4303–417. https://doi.org/10.1021/cr030203g.
[38] Xiong DJ, Bauer M, Ellis LD, Hynes T, Hyatt S, Hall DS, et al. Some Physical Properties of Ethylene Carbonate-Free Electrolytes. J Electrochem Soc 2018;165:A126–31. https://doi.org/10.1149/2.0511802jes.
[39] Xu K. Electrolytes and interphases in Li-ion batteries and beyond. Chem Rev 2014;114:11503–618. https://doi.org/10.1021/cr500003w.
[40] Von Wald Cresce A, Borodin O, Xu K. Correlating Li+ solvation sheath structure with interphasial chemistry on graphite. J Phys Chem C 2012;116:26111–7. https://doi.org/10.1021/jp303610t.
[41] Logan ER, Tonita EM, Gering KL, Li J, Ma X, Beaulieu LY, et al. A Study of the Physical Properties of Li-Ion Battery Electrolytes Containing Esters. J Electrochem Soc 2018;165:A21–30. https://doi.org/10.1149/2.0271802jes.
[42] Ue M, Mori S. Mobility and Ionic Association of Lithium Salts in a Propylene Carbonate-Ethyl Methyl Carbonate Mixed Solvent. J Electrochem Soc 1995;142:2577–81. https://doi.org/10.1149/1.2050056.